GeoPlanning

Journal of Geomatics and Planning

Geoplanning: Journal of Geomatics and Planning, Vol. 13, No. 1, 2026, 35 - 60

e-ISSN: 2355-6544

Received: 26 December 2025;
Revised: 26 May 2026;
Accepted: 31 May 2025;
Available Online: 12 June 2026;
Published: 15 June 2026.

Keywords:
Flood Risk Assessment, Bivariate Hazard-Vulnerability Matrix, Mitigation Prioritization, Geospatial Modeling

*Corresponding author(s)
email: hasannugraha791@gmail.com

Original Research Open access

Integrated Flood Risk Mapping and Hazard-Vulnerability Assessment for Mitigation Prioritization in Sumatra

Hasan Adi Nugraha[1,2,3]*, M. Angga Hadi Pratama[1,4], Muhammad Alsamtu Tita Sabila Pratama Suhartono[5], Anjar Dimara Sakti[2,3], Ketut Wikantika[2,3]

1. *Geodesy and Geomatics Engineering Postgraduate Program, Faculty of Earth Sciences and Technology, Institut Teknologi Bandung, Bandung, Indonesia*
2. *Remote Sensing and Geographic Information Sciences Research Group, Faculty of Earth Sciences and Technology, Institut Teknologi Bandung, Bandung, Indonesia*
3. *Center for Remote Sensing, Institut Teknologi Bandung, Bandung, Indonesia*
4. *Geodetic Science, Engineering, and Innovation Research Group, Faculty of Earth Sciences and Technology, Institut Teknologi Bandung, Bandung, Indonesia*
5. *Graduate School of International Resource Science, Faculty of International Resource Science, Akita University, Akita, Japan*

DOI: 10.14710/geoplanning.13.1.35-60

Abstract

Flood risk in tropical regions such as Sumatra is increasing due to intensified rainfall extremes and rapid urbanization. Although flood hazard mapping is widely applied, many studies do not clearly distinguish physical hazard from socio-economic vulnerability, limiting their usefulness for targeted mitigation. This study proposes an integrated geospatial framework combining multi-parameter flood hazard assessment and a socio-demographic vulnerability index through a bivariate hazard–vulnerability matrix to support risk reduction. The framework was applied to the November 2025 flood events in Aceh, North Sumatra, and West Sumatra, using nine hazard parameters and four vulnerability indicators. Results show that High to Very High Hazard zones cover 21% of the study area, in lowland basins, while 12% of the area falls into the Very High-Risk category. Validation using observed damage data shows that medium-risk (Risk 2) zones, rather than only the highest-risk cores, account for 87.5%–100% of the exposed population across five major cities, capturing 97.5% of affected residents in Aceh Tamiang. The proposed 5×5 bivariate matrix separates risk dominated by physical hazard, socio-economic vulnerability, or their interaction This enables stratified mitigation strategies, ranging from integrated structural and social interventions to targeted engineering and community-based measures, while providing spatially explicit guidance to strengthen flood risk management and support Sendai Framework objectives under climate change.

1. Introduction

Floods are among the most frequent hydrometeorological disasters worldwide (Ferreira, 2020). They continue to generate substantial social impacts such as mass displacement and economic disruption which increase pressure on disaster management systems (Bui et al., 2019; Taoukidou et al., 2025). Over recent decades, global flood risk has intensified, driven by rapid population growth, uncontrolled urban expansion, and climate change, which amplifies the frequency and intensity of extreme weather events (IPCC, 2023; Tellman et al., 2021). In developing countries such as Indonesia, floods consistently represent the dominant disaster type, reflecting the combined influence of physical environmental conditions and high levels of social vulnerability (Aeni & Anwar, 2024; Ramadhan et al., 2022).

Within contemporary disaster risk research, flood risk is commonly conceptualized as the interaction between hazard and vulnerability, often complemented by the dimension of exposure. This framework emphasizes that flood impacts are not determined solely by the magnitude of physical hazards, but by the way these hazards interact with the social, demographic, and economic characteristics of exposed communities (Arrighi et al., 2021; Islam et al., 2025; Parizi et al., 2022). This interaction becomes increasingly complex in the context of consecutive disasters, where previous events can exacerbate existing vulnerabilities and constrain recovery capacity (de Ruiter et al., 2020). Consequently, a comprehensive understanding of flood risk requires the explicit identification and systematic analysis of hazard and vulnerability components prior to their spatial integration.

The hazard component of flood risk is typically represented by a set of physical and hydromorphological parameters that govern the generation and propagation of inundation. Numerous GIS-based studies have demonstrated the critical role of topographic factors, such as elevation and slope, in determining flood hazard (Ahmed et al., 2024; Saha et al., 2021). Furthermore, hydrological features and land-use characteristics are also widely recognized as key determinants of these spatial patterns (Ali et al., 2019; Ariyani et al., 2024). GIS-based multi-parametric approaches, particularly those employing the Analytical Hierarchy Process (AHP), have been widely applied to integrate these parameters into flood hazard zonation maps in a transparent and structured manner (Ibrahim et al., 2024; Sakti et al., 2024). Among the hazard parameters, extreme rainfall plays a critical role as the primary trigger and an important amplifying factor, especially when interacting with low-lying topography and limited drainage capacity (IPCC, 2023; Ramadhan et al., 2022). Rainfall is therefore positioned as an integral element of the hazard component rather than as an independent driver within flood risk analysis.

In addition to conventional AHP-based approaches, several studies have emphasized the importance of methodological comparison to enhance the robustness of flood hazard assessments. Comparative analyses using AHP, Fuzzy AHP, and Frequency Ratio methods have demonstrated that incorporating uncertainty handling and data-driven techniques can improve the reliability of hazard zonation results (Ekmekcioğlu et al., 2021; Nguyen et al., 2023; Parsian et al., 2021; Taoukidou et al., 2025). These methodological developments highlight the evolving nature of flood hazard modelling and underscore the need for careful parameter weighting and validation.

In contrast, the vulnerability component reflects the susceptibility of populations and assets to flood impacts. Vulnerability is commonly represented through multidimensional indicators such as population size and density, age structure, socio-economic conditions, and the characteristics of settlements and buildings (Asaaga et al., 2023; Gomez Vaca et al., 2025; Rahman et al., 2025). Recent conceptual analyses emphasize that vulnerability is not merely the inverse of resilience, but a distinct state shaped by historical, institutional, and systemic factors (Lanlan et al., 2024; Verma et al., 2025). Empirical evidence shows that areas exposed to similar levels of flood hazard may experience substantially different numbers of affected people and evacuees due to variations in social vulnerability and adaptive capacity (Arrighi et al., 2021; Tellman et al., 2021). Furthermore, the physical characteristics of the built environment, such as building properties and infrastructure resilience, play a significant role in determining the magnitude of physical damage (Leal et al., 2021). This highlights the critical role of vulnerability analysis in explaining the uneven spatial distribution of flood impacts.

The integration of hazard and vulnerability components is commonly operationalized through flood risk mapping. Such maps are widely developed using Geographic Information Systems (GIS) combined with Multi-Criteria Decision Analysis (MCDA) techniques, particularly AHP (Ariyani et al., 2024; Sakti et al., 2024). These combined methods effectively enable the aggregation of diverse physical and social indicators into a single spatial risk index (Diriba et al., 2024; Dulawan et al., 2024). Recent studies have further demonstrated the value of utilizing open-access spatial data for flood risk mapping, particularly in data-scarce regions, to enhance transparency, reproducibility, and operational applicability (Jumadi et al., 2024). However, many flood risk studies remain limited to the production of composite risk maps without explicitly examining the relative contributions of hazard and vulnerability in shaping observed risk patterns.

The validity of social vulnerability models often depends on the accuracy of the underlying metrics and their sensitivity to local conditions (Rufat et al., 2019). This limitation can obscure important differences in risk characteristics, as areas with similar overall risk levels may be driven by fundamentally different mechanisms, either dominant physical hazards or high levels of social vulnerability (Islam et al., 2025). This gap underscores the need for analytical approaches that move beyond composite indices to disentangle the respective roles of hazard and vulnerability.

While previous flood risk studies have widely utilized composite hazard and vulnerability indices, fewer studies have explicitly differentiated the dominant spatial drivers of flood risk for mitigation prioritization at regional scales. In highly heterogeneous regions such as Sumatra, areas with similar composite risk values may nevertheless be influenced by substantially different combinations of physical hazard intensity and socio-economic vulnerability. Therefore, improving the interpretability of flood risk patterns through explicit hazard–vulnerability differentiation may provide additional value for context-specific and operationally targeted mitigation planning.

Bivariate approaches that jointly analyze hazard and vulnerability have increasingly been recognized as effective tools to address this limitation. By explicitly examining the interaction between these two components, bivariate analyses enable the identification of dominant risk drivers and support more targeted and context-specific mitigation strategies (Arrighi et al., 2021). Beyond methodological considerations, the empirical validation of flood risk maps against observed impacts remains relatively limited. In people-centered flood risk assessments, data on affected populations and evacuees represent critical indicators that capture real-world interactions among hazard, vulnerability, and exposure, while also holding direct relevance for disaster response and policy decisions (Asaaga et al., 2023; Tellman et al., 2021).

To address these gaps, this study advances beyond standard composite risk mapping by offering an empirically validated, operational decision-support framework. The primary methodological contribution of this research lies in two key areas. First, it rigorously bridges theoretical modeling with empirical reality by validating the spatial risk model against ground-truth displacement data from the catastrophic November 2025 event. Second, it operationalizes risk data by systematically aggregating a complex 25-class bivariate hazard-vulnerability matrix into five actionable mitigation priority zones. By doing so, this study provides a replicable methodological pathway to transform diagnostic risk assessments into targeted, context-specific disaster risk reduction strategies.

2. Data and Methods

2.1. Study Area

The study area covers three provinces on the island of Sumatra, namely Aceh, North Sumatra, and West Sumatra, which were directly affected by a major flood event in late November 2025, as documented in official disaster reports from Indonesia's National Disaster Management Agency (BNPB) and the European Commission (BNPB, 2025; European Commission, 2025) (see Figure 1). Physiographically, the region is characterized by the Bukit Barisan mountain range and adjacent lowland areas, with river systems draining from upstream catchments toward downstream settlements. This topographic and hydrological configuration increases susceptibility to fluvial flooding during periods of intense rainfall, particularly in densely populated urban lowland areas.

During the November 2025 event, heavy rainfall triggered river overflow and widespread inundation across multiple locations in the three provinces (European Commission, 2025; IPCC, 2023). Accordingly, Aceh, North Sumatra, and West Sumatra were selected as the study area to represent the spatial patterns of flood risk during the November 2025 flood event, analyzed using a hazard and vulnerability based framework.

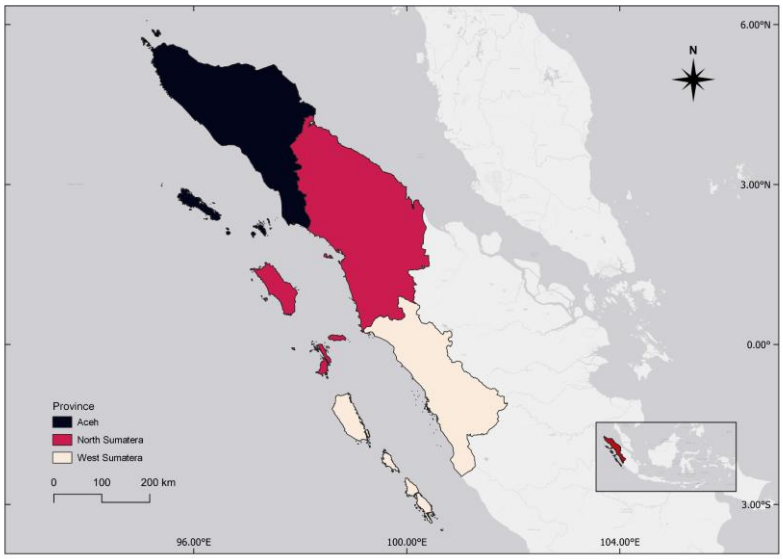

Figure 1. Area of Study

2.2. Data

This study utilizes a range of open-access spatial and statistical datasets to characterize flood hazard, vulnerability, and exposure across the study area. The data encompass topographic, hydrometeorological, land surface, and socio-economic information obtained from widely used global and national sources, including satellite-derived products and official statistics. All datasets were standardized to a common spatial resolution of 90 × 90 m based on the SRTM Digital Elevation Model to ensure spatial consistency and compatibility for subsequent raster-based analyses. A summary of the data sets used, along with their sources and characteristics, is provided in Table 1.

Table 1. Data Used for Hazard and Vulnerability Assessment

Data	Product	Provider	Type	Year
Elevation	Digital Elevation Model (DEM)	NASA / USGS	Raster	-
Slope	Slope (derived from DEM)	Derived from DEM	Raster	-
Flow Accumulation	Flow Accumulation (derived from DEM)	Derived from DEM	Raster	-
Profile Curvature	Profile Curvature (derived from DEM)	Derived from DEM	Raster	-
Topographic Wetness Index	TWI (derived from DEM)	Derived from DEM	Raster	-
Land Use / Land Cover	Global Land Use Land Cover	ESRI	Raster	2025
Distance from River	River network & Euclidean distance	OpenStreetMap	Vector	2024
Rainfall	CHIRPS Precipitation Dataset	Climate Hazards Group	Raster	2020-2025
Soil Type	Digital Soil Map of the World	FAO	Raster	-
Population by Age	Population by age group (district/city)	BPS Indonesia	Tabular	2024
Total Population	Total population (district/city)	BPS Indonesia	Tabular	2024
Building Volume	Global Human Settlement Layer – Built Volume	European Commission (JRC)	Raster	2025
Urbanization	Degree of Urbanization	European Commission (JRC)	Raster	2025
Disaster Loss Data	Flood damage statistics	BNPB Indonesia	Tabular	2025

Source: Analysis, 2025

2.3. Flood Hazard Assessment

Flood hazard was assessed using a GIS-based multi-parameter framework that integrates topographic, hydrological, environmental, and climatic variables widely recognized as primary controls of flood occurrence and spatial extent. This framework enables an explicit representation of spatial heterogeneity in flood-prone conditions and has been extensively applied in recent flood hazard and risk mapping studies (Ahmed et al., 2024; Jumadi et al., 2024; Pakati et al., 2025; Taoukidou et al., 2025). Each hazard parameter was derived from spatial datasets, reclassified into five hazard levels ranging from very low to very high, and standardized prior to integration. The spatial distribution of individual hazard parameter scores is presented in Figure 2.

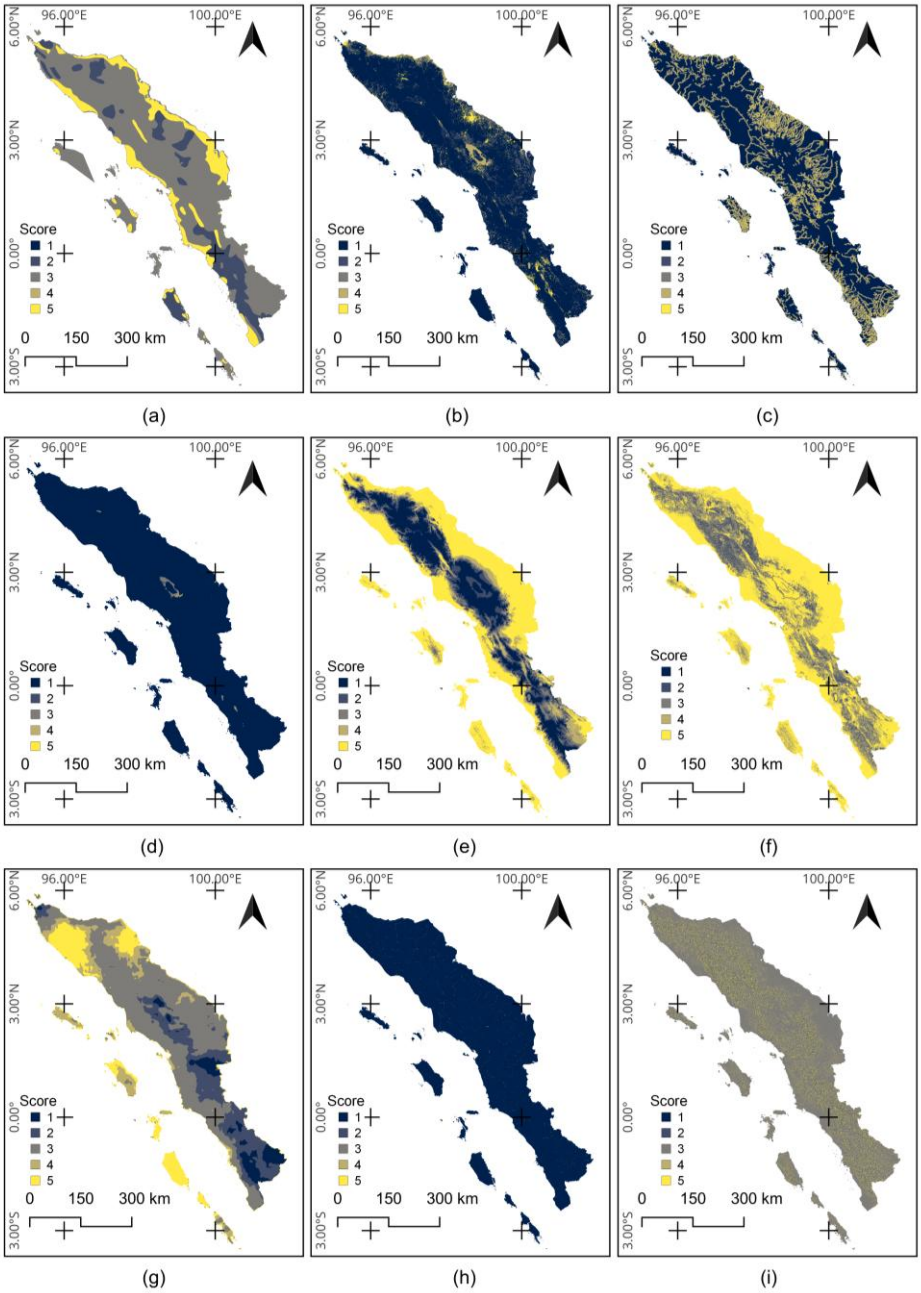

Figure 2. Visualized Score of Individual Hazard Parameters: (a) Soil, (b) LULC, (c) Distance from River, (d) TWI, (e) DEM, (f) Slope, (g) Rainfall, (h) Flow Accumulation, (i) Profile Curvature

2.3.1. Elevation

Elevation plays a critical role in controlling surface runoff concentration, floodplain development, and river overflow dynamics. Low-lying areas are generally more susceptible to flooding due to reduced gravitational drainage and prolonged water retention during extreme rainfall events (Purwanto et al., 2022; Saha et al., 2021). The elevation layer was derived from the Shuttle Radar Topography Mission (SRTM) Digital Elevation Model and classified into five hazard classes. As shown in Figure 2e, lower elevation zones were assigned to higher flood hazard scores, while higher elevation areas were classified into lower hazard levels, following thresholds commonly adopted in recent regional flood hazard studies (Ahmed et al., 2024; Jumadi et al., 2024).

2.3.2. Slope

Slope influences runoff velocity, infiltration capacity, and the potential for water accumulation. Areas characterized by gentle slopes tend to favor ponding and floodplain inundation, whereas steeper slopes promote rapid runoff and shorter flood residence times (Ahmed et al., 2024). Slope was derived from the digital elevation model as the maximum rate of elevation change between each grid cell and its neighboring cells, as illustrated in Figure 2f. In this study, lower slope values were assigned higher flood hazard scores due to their stronger association with floodwater accumulation, consistent with recent GIS-based flood hazard assessments (Ahmed et al., 2024; Taoukidou et al., 2025).

2.3.3. Flow Accumulation

Flow accumulation represents the cumulative contribution of upstream grid cells draining surface runoff into a given cell and serves as a proxy for runoff convergence and channelized flow. Areas characterized by high flow accumulation are more susceptible to flooding due to increased discharge concentration (Ahmed et al., 2024; Ali et al., 2019). The flow accumulation layer, shown in Figure 2h. Higher flow accumulation values were classified into higher hazard levels, following recent flood susceptibility and hazard mapping studies that integrate hydrological parameters (Ahmed et al., 2024; Jumadi et al., 2024).

2.3.4. Profile Curvature

Profile curvature describes terrain curvature along the direction of maximum slope and influences flow acceleration and deceleration processes. Negative profile curvature values indicate concave surfaces that promote flow convergence and water accumulation, whereas positive values represent convex surfaces that encourage flow divergence (Ahmed et al., 2024; Saha et al., 2021). Profile curvature was visualized in Figure 2i.. In this study, areas characterized by concave profile curvature were assigned higher flood hazard scores due to their enhanced capacity for runoff retention, consistent with geomorphology-based flood hazard assessments (Ahmed et al., 2024; Jumadi et al., 2024).

2.3.5. Topographic Wetness Index

The Topographic Wetness Index (TWI) characterizes the spatial distribution of potential soil moisture and saturation conditions by integrating upslope contributing area and local slope. Higher TWI values indicate locations prone to water accumulation and prolonged saturation (Parizi et al., 2022; Parsian et al., 2021). The TWI layer shown in Figure 2d. Areas with higher TWI values were classified into higher flood hazard categories, in line with recent GIS-based flood hazard studies conducted in tropical and subtropical environments (Ahmed et al., 2024; Taoukidou et al., 2025).

2.3.6. Land Use/Land Cover

Land use and land cover strongly influence flood hazard by regulating infiltration capacity, surface roughness, and runoff generation. Built-up and agricultural areas generally exhibit higher runoff potential due to impervious surfaces and soil compaction, whereas forested areas enhance infiltration and attenuate surface flow (Ibrahim et al., 2024). The spatial distribution of land use and land cover hazard scores is illustrated in

Figure 2b. Land use and land cover classes were reclassified into five hazard levels, with higher scores assigned to built-up and intensively cultivated areas, following recent flood hazard and risk mapping studies (Ahmed et al., 2024; Ariyani et al., 2024; Jumadi et al., 2024).

2.3.7. Distance from River

Proximity to river channels represents a direct indicator of exposure to fluvial flooding caused by river overflow. Areas located closer to river networks are more likely to experience inundations during high-discharge events. Distance from river networks was calculated using the Euclidean distance function, and the resulting spatial pattern is shown in Figure 2c. Areas situated closer to rivers were assigned higher flood hazard scores, consistent with recent flood hazard zonation studies (Ahmed et al., 2024; Saha et al., 2021; Taoukidou et al., 2025).

2.3.8. Soil

Soil properties influence flood hazard through their control on infiltration rates and runoff generation. Poorly drained and hydromorphic soils tend to promote surface ponding and rapid runoff accumulation (Ali et al., 2019). The soil hazard parameter, visualized in Figure 2a, was derived from soil classification data and reclassified into five hazard levels. Poorly drained soils were assigned high to very high hazard scores, following recent flood hazard assessments incorporating soil drainage characteristics (Ahmed et al., 2024; Megahed et al., 2023).

2.3.9. Rainfall

Rainfall intensity and spatial distribution constitute the primary triggering mechanism of flood events, particularly under changing climatic conditions that intensify extreme precipitation. Spatial rainfall distribution was derived from CHIRPS data and classified into five hazard levels, with higher rainfall amounts assigned higher hazard scores, as shown in Figure 2g. Although rainfall represents one of several hazard parameters, its inclusion captures the dynamic forcing that initiates flooding, particularly during extreme events (IPCC, 2023; Jumadi et al., 2024; Ramadhan et al., 2022; Taoukidou et al., 2025).

2.3.10. Composite Flood Hazard Index

The composite flood hazard index was generated using a weighted linear combination approach. Each hazard parameter was standardized to a common scale ranging from 1, representing very low hazard, to 5, representing very high hazard, as presented in Table 2. The composite flood hazard index was calculated using Equation 1, expressed as:

$$H = \sum_{i=1}^{n} w_i \cdot h_i \quad \text{..... (Equation 1)}$$

where H denotes the composite flood hazard index, h_i represents the standardized score of the i-th hazard parameter, w_i corresponds to the weight assigned to that parameter, and $n$indicates the total number of hazard parameters included in the analysis.

The parameters comprise elevation, slope, flow accumulation, profile curvature, topographic wetness index, land use and land cover, distance from river, soil, and rainfall. Parameter weights were adopted from recent GIS-based flood hazard studies employing the Analytical Hierarchy Process and related multi-criteria decision-making frameworks (Ahmed et al., 2024; Bui et al., 2019; Jumadi et al., 2024; Nguyen et al., 2023; Taoukidou et al., 2025). The adopted weighting configuration was intended to provide a generalized regional-scale representation of flood hazard conditions across Sumatra based on commonly applied parameter importance reported in previous studies. However, given the substantial environmental and hydrological heterogeneity of the study area, the relative influence of individual hazard parameters may vary across local contexts. Consequently, the selected weights should be interpreted as representative approximations rather than universally calibrated parameter importance values.

Table 2. Score and Weight of Hazard Parameters

Parameters	Values	Degree of Flood Hazard	Score	Weight (%)
Elevation (m)	<62	Very High	5	20
	62 – 104	High	4	
	104 – 166	Moderate	3	
	166 – 250	Low	2	
	>433	Very Low	1	
Slope	0 – 9	Very High	5	17
	9 – 19	High	4	
	19 – 33	Moderate	3	
	33 – 61	Low	2	
	>61	Very Low	1	
Flow Accumulation	>95,277	Very High	5	17
	39,829 – 95,277	High	4	
	17,181 – 39,829	Moderate	3	
	3,904 – 17,181	Low	2	
	<3,904	Very Low	1	
Profile Curvature	>0.67	Very High	5	2
	0.13 – 0.67	High	4	
	-0.32 – 0.13	Moderate	3	
	-0.87 – -0.32	Low	2	
	<-0.87	Very Low	1	
Topographic Wetness Index (TWI)	>12.45	Very High	5	7
	9.56 – 12.45	High	4	
	7.51 – 9.56	Moderate	3	
	5.99 – 7.51	Low	2	
	<5.99	Very Low	1	
LULC	Settlement	Very High	5	8
	Agricultural Land	High	4	
	Open Forest	Moderate	3	
	Dense Forest	Low	2	
	Water Body	Very Low	1	
Distance from River (km)	<2	Very High	5	12
	2 – 4	High	4	
	4 – 6	Moderate	3	
	6 – 8	Low	2	
	>8	Very Low	1	
Soil	Hydromorphic	Very High	5	5
	Poorly drained	High	4	
	Moderately drained	Moderate	3	
	Well-drained	Low	2	
	Rapid drainage	Very Low	1	
Rainfall (mm)	>621	Very High	5	12
	532 – 621	High	4	
	354 – 532	Moderate	3	
	265 – 354	Low	2	
	<265	Very Low	1	

Source: Analysis, 2025

2.4. Flood Vulnerability Assessment

Flood vulnerability was assessed by integrating demographic, socio-spatial, and built-environment indicators that represent the susceptibility of exposed populations and assets to flood impacts. Vulnerability

parameters were selected based on recent flood risk literature emphasizing population concentration, demographic sensitivity, urban development intensity, and the physical exposure of built structures (de Ruiter et al., 2020; Dulawan et al., 2024; Rufat et al., 2019). Each parameter was spatially derived, standardized into five vulnerability levels ranging from very low to very high, and subsequently integrated into a composite vulnerability index (Gomez Vaca et al., 2025; Rahman et al., 2025). The spatial distribution of individual vulnerability parameter scores is illustrated in Figure 3.

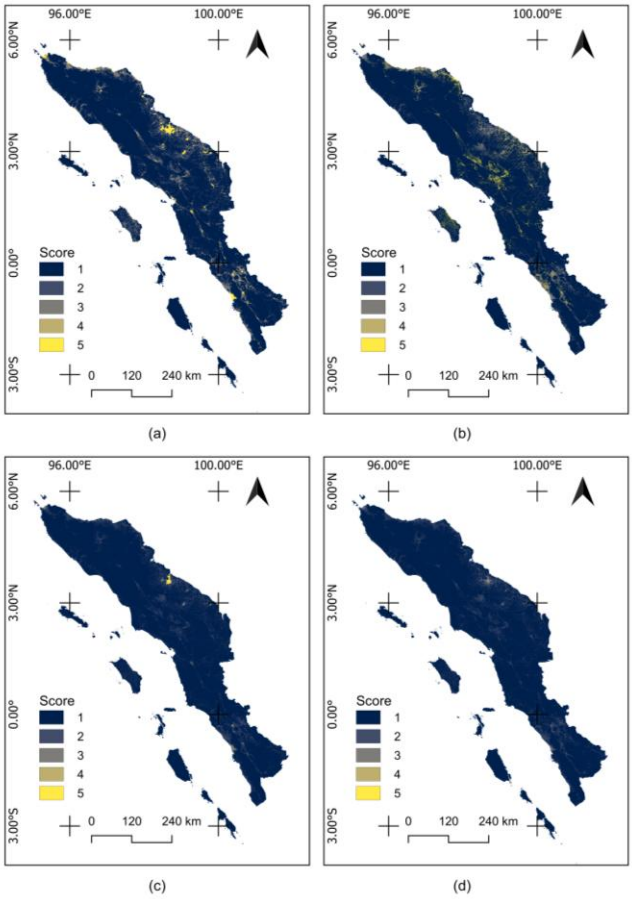

Figure 3. Visualized Score of Individual Parameters: (a) Urbanization, (b) Age Vulnerability, (c) Population, (d) Building Volume

2.4.1. Population

Population density was used to represent exposure concentration (Dulawan et al., 2024; Tellman et al., 2021). Population vulnerability was quantified as population per grid cell within settlement areas. Because population data were available only at the regency and municipal levels, an areal-weighted disaggregation approach was applied, which has been widely adopted in recent large-scale flood risk assessments (de Ruiter et al., 2020; Jumadi et al., 2024). This approach provides a practical solution for regional-scale exposure assessment where high-resolution demographic data are unavailable. Nevertheless, the uniform distribution of population across settlement grids represents a simplifying assumption that may not fully capture localized variations in settlement density, particularly within heterogeneous urban and peri-urban environments.

For each administrative unit, the total settlement area was divided by the grid cell area to determine the number of settlement grids, and the total population was then evenly distributed across these grids. Population per grid cell (P_{grid}) was calculated using Equation 2, expressed as

$$P_{grid} = \frac{P_{total}}{N_{settlement}} \text{ ..... (Equation 2)}$$

where P_{total} represents the total population of a regency or city and $N_{settlement}$ denotes the number of grid cells classified as settlement land use within that administrative unit.

Grid cells outside settlement areas were assigned to Class 1 (unclassified). The resulting population density values were classified into five vulnerability levels according to the thresholds presented in Table 3, and the spatial pattern of population vulnerability is shown in Figure 3c.

2.4.2. Degree of Urbanization

The degree of urbanization was used as a proxy for development intensity and the concentration of people and assets exposed to flooding. Differences in urbanization levels correspond to variations in flood vulnerability, as densely urbanized areas generally experience higher impacts due to dense populations, extensive impervious surfaces, and complex infrastructure networks (Islam et al., 2025; Verma et al., 2025). This spatial variation is illustrated in Figure 3a, which shows the distribution of urban exposure across the study area. Urbanization data derived from the Global Human Settlement Layer were classified into urban center, dense urban, suburban, and rural categories to represent the multidimensional nature of urban exposure (Gomez Vaca et al., 2025; Lanlan et al., 2024).

2.4.3. Age Vulnerability Index

Demographic structure was included to represent age-related vulnerability differences (Rahman et al., 2025; Rufat et al., 2019). Age-related vulnerability was assessed using an Age Vulnerability Index (AVI) that accounts for differences in flood sensitivity across age groups, consistent with recent disaster vulnerability frameworks (Dulawan et al., 2024; Gomez Vaca et al., 2025). The AVI was calculated using Equation 3,

$$AVI = \frac{(P_c \cdot w_c)+(P_w \cdot w_w)+(P_e \cdot w_e)}{P_{total}} \text{ ..... (Equation 3)}$$

where P_{total} is total population, P_c, P_w, and P_e represent population counts in each age group, and w_c, w_w, and w_e are vulnerability weights set to 5, 2.3, and 5, respectively, reflecting vulnerability among children and elderly.

Population data were divided into three age categories: children (<15 years), working-age population (15–64 years), and elderly (>64 years). The resulting AVI values were classified into five vulnerability classes using a standard deviation-based classification scheme (Gomez Vaca et al., 2025; Rahman et al., 2025), and the spatial distribution of age-related vulnerability is shown in Figure 3b.

2.4.4. Building Volume

Building volume represented physical exposure. Higher building volumes reflect greater concentrations of built assets and infrastructure, which are commonly associated with increased economic losses and complex post-flood recovery processes (Arrighi et al., 2021; Leal et al., 2021). As illustrated in Figure 3d, areas with high building volume exhibit higher vulnerability levels. Building volume data were obtained from the Global Human Settlement Layer, while non-settlement grids were categorized as unclassified (Class 1). Higher building volume values were assigned to greater vulnerability scores and subsequently classified into five vulnerability levels based on the thresholds and weighting scheme (see Table 3) (Ahmed et al., 2024; Parizi et al., 2022).

2.4.5. Composite Vulnerability Index

The composite flood vulnerability index (V) was calculated by integrating all vulnerability parameters using a weighted linear combination approach. Each parameter was standardized to a common scale ranging

from 1, representing very low vulnerability, to 5, representing very high vulnerability. The composite vulnerability index was calculated using Equation 4, expressed as

$$V = \sum_{i=1}^{n} w_i \cdot v_i \text{ ..... (Equation 4)}$$

where v_i represents the standardized score of each vulnerability parameter, including population, degree of urbanization, age vulnerability index, and building volume, and w_i denotes the corresponding parameter weight as shown in Table 3.

Table 3. Score and Weight of Vulnerability Parameters

Parameters	Values	Degree of Flood Vulnerability	Score	Weight (%)
Population	>62	Very High	5	30
	41 – 62	High	4	
	21 – 41	Moderate	3	
	1 – 21	Low	2	
	0	Very Low	1	
Degree of Urbanization	Urban Center	Very High	5	20
	Dense Urban	High	4	
	Sub-Urban	Moderate	3	
	Rural	Low	2	
	Unclassified	Very Low	1	
Age Vulnerability Index	3.232 – 3.313	Very High	5	30
	3.185 – 3.232	High	4	
	3.138 – 3.185	Moderate	3	
	3.117 – 3.138	Low	2	
	Unclassified	Very Low	1	
Building Volume	>61,965	Very High	5	20
	41,310 – 61,965	High	4	
	20,655 – 41,310	Moderate	3	
	1 – 20,655	Low	2	
	0	Very Low	1	

Source: Analysis, 2025

Similar to the flood hazard assessment, the weighting configuration used in the vulnerability index was intended to provide a generalized regional-scale representation of vulnerability conditions across Sumatra based on commonly applied parameter importance reported in previous flood vulnerability studies. Nevertheless, vulnerability patterns are inherently influenced by local socio-economic characteristics, settlement structures, and adaptive capacity. Therefore, the resulting vulnerability index should be interpreted as a relative spatial representation of vulnerability conditions rather than as a fully calibrated measure of societal flood susceptibility (Ahmed et al., 2024; Dulawan et al., 2024; Gomez Vaca et al., 2025).

2.5. Flood Risk Mapping

The flood risk index was generated using a multiplicative approach to integrate the hazard (H) and vulnerability (V) indices (Ahmed et al., 2024). This method is widely utilized because it explicitly reflects the complex interaction between physical hazard intensity and societal susceptibility (Ekmekcioğlu et al., 2021; Jumadi et al., 2024). This conceptualization is consistent with contemporary disaster risk frameworks, in which risk is understood as the product of physical threats and the vulnerability of exposed systems (de Ruiter et al., 2020; IPCC, 2023). Prior to integration, both indices were standardized to a common ordinal scale ranging from 1, representing very low, to 5, representing very high. The flood risk index (R) was calculated using the multiplicative formulation presented in Equation 5. This formulation ensures that high flood risk values occur

only in locations where both hazard and vulnerability are elevated, thereby facilitating the identification of spatial areas where elevated hazard intensity and socio-economic vulnerability potentially interact to produce higher flood risk conditions (Gomez Vaca et al., 2025; Islam et al., 2025).

$$R = H \times V \text{ ..... } \textit{(Equation 5)}$$

where H represents the composite flood hazard index and V denotes the composite flood vulnerability index for each grid cell.

The resulting flood risk values were subsequently classified into five flood risk classes, very low, low, moderate, high, and very high to facilitate spatial interpretation and comparison across the study area. This classification scheme supports decision-making by prioritizing regions where mitigation measures and adaptive capacity building are most urgently required (Dulawan et al., 2024; Rahman et al., 2025; Verma et al., 2025). Furthermore, this integrated approach supports a more differentiated interpretation of how spatial flood risk patterns may be influenced by the relative dominance of physical hazards and socio-economic vulnerability (Arrighi et al., 2021; Rufat et al., 2019).

2.6. Research Flow Chart

Figure 4 illustrates the overall workflow in this study, including flood hazard, vulnerability, and risk assessment, and the development of a mitigation framework. The process starts with data collection and preprocessing, to ensure reliable input for hazard, and vulnerability assessment. The outputs of these two assessments are then integrated to perform a flood risk assessment. This section of workflow generates flood hazard, vulnerability, and risk maps. Furthermore, the flood risk assessment results are utilized to develop mitigation framework. A hazard–vulnerability matrix analysis is performed to identify mitigation priority zones, which are further evaluated through population exposure analysis. To ensure a trusted and reliable model, ground-truth validation is then conducted. Finally, the validated results are synthesized into a comprehensive flood mitigation framework that supports effective disaster risk reduction and planning strategies.

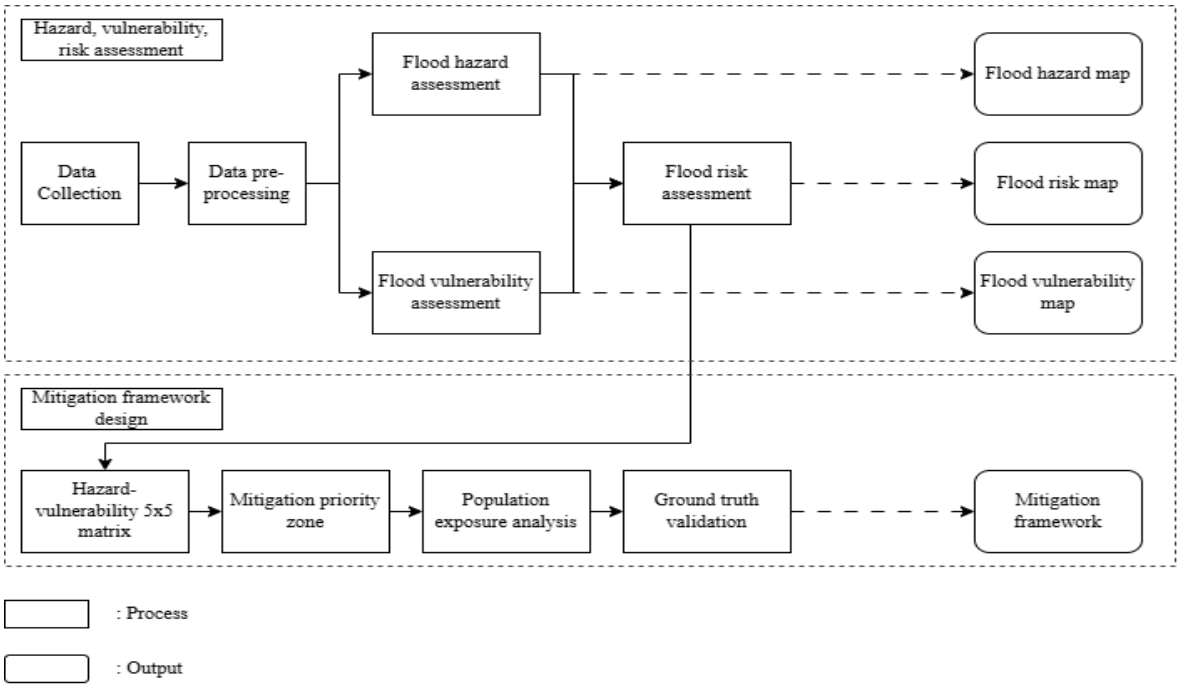

Figure 4. Research Flow Chart

3. Results and Discussion

3.1. Flood Hazard and its Spatial Distribution

The flood hazard map (see Figure 5) delineates five hazard levels derived from nine physical parameters, with High and Very High Hazard zones constituting 21% of the study area and concentrated in lowland river basins and coastal plains. This spatial pattern demonstrates a direct correlation with peak rainfall anomalies recorded during the November 2025 event, aligning with established geomorphic flood hazard mapping approaches that emphasize rainfall–topography interactions (Magnini et al., 2023). Low and very low hazard zones correspond to upland regions with steep topography and lower rainfall totals. These findings align established geomorphological principles where elevation and slope are primary controls on flood inundation. The concentration of high hazard in low-lying areas underscores the persistent vulnerability of these landscapes to fluvial and pluvial flooding, a pattern documented in similar tropical environments.

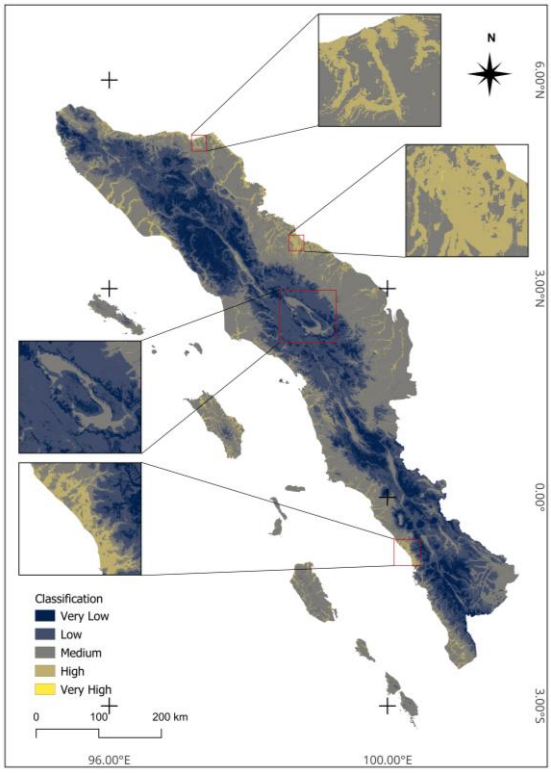

Figure 5. Flood Hazard Map of the Study Area

The human dimension and tangible impacts of this modeled hazard are starkly illustrated in Figure 6. The photographs document the severe social consequences of the November 2025 floods across multiple provinces, including Aceh Tamiang, North Aceh, and South Tapanuli regions identified as high-hazard zones in our model. Scenes of displaced residents queuing for aid in Kuala Cangkoy, salvaging belongings in Kuala Simeulue, and taking shelter in warehouses in Batang Toru (South Tapanuli) provide a poignant ground-truth validation of the hazard map's predictions. This visual evidence confirms that the modeled physical hazard zones are not abstract GIS layers but landscapes where real communities face profound disruption, loss of shelter, and dependency on emergency relief, echoing findings on social vulnerability and community reliance in Aceh flood contexts (Santi et al., 2022).

Furthermore, the spatial concentration of high hazard in low-lying areas highlights a persistent and systemic vulnerability within these landscapes. The integration of multi-parameter modeling including factors

such as flow accumulation, soil drainage, and land use reveals that these zones are not only susceptible due to topography but also due to compounded environmental sensitivities. For instance, areas with high flow accumulation and low drainage efficiency exhibit significantly higher hazard scores, indicating a convergence of multiple flood-inducing factors. This multi-criteria approach enhances the robustness of the hazard assessment, moving beyond single-parameter analyses to capture the complex interplay of environmental variables that drive flood inundation. The methodological alignment with established frameworks, such as the Analytical Hierarchy Process (AHP) and weighted linear combination, ensures that the hazard model is both replicable and scalable, suitable for application in other data-scarce tropical regions.

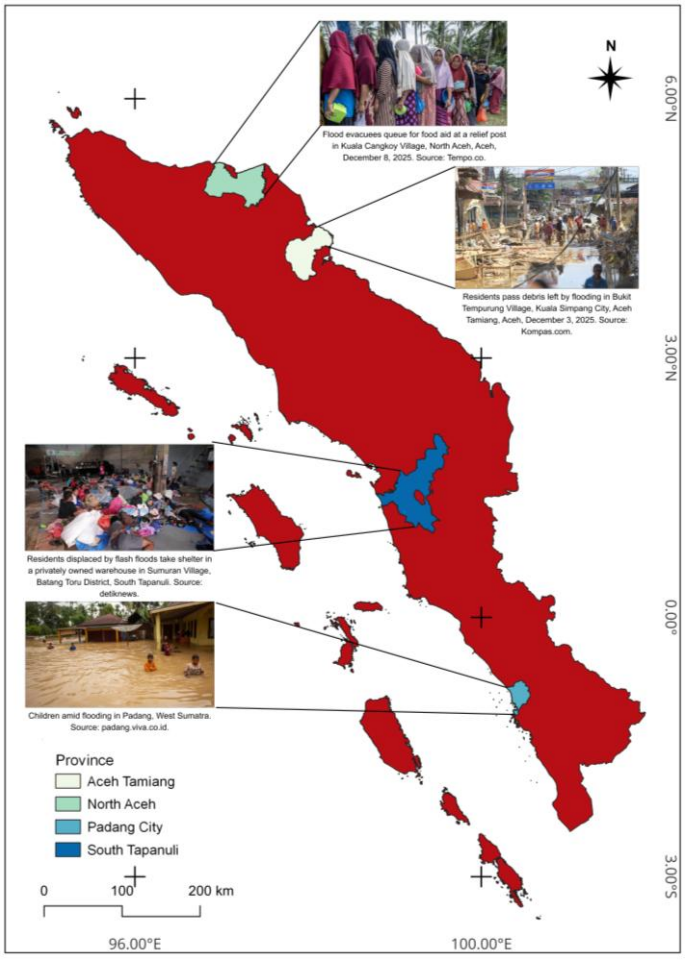

Figure 6. Spatial Distribution of Flood Events and Affected Risk Zones in Sumatra

3.2. *Socio-Economic Vulnerability to Flooding* Hazard

The vulnerability assessment, based on four socio-economic parameters, resulted in a map classified into five levels (see Figure 7). 'Very High' and 'High' vulnerability districts are clustered around major urban centers and densely populated agricultural zones. These areas are characterized by a confluence of high population density (>1500 persons/km^2), elevated proportions of children and elderly (>25%), and lower access to resilient infrastructure. This pattern highlights a critical dimension of flood risk: physical exposure is compounded by social fragility, consistent with recent findings that socio-demographic characteristics strongly influence vulnerability in Indonesian flood-prone regions (Istiawan et al., 2023; Sigit et al., 2023). The high proportion of dependent age groups (children and elderly) in these zones significantly increases sensitivity and reduces adaptive capacity, a vulnerability factor emphasized in contemporary disaster risk literature (Mondal & Garg,

2025). This result suggests that mitigation strategies must address not only physical hazard but also the underlying socio-economic conditions that transform a natural event into a human disaster.

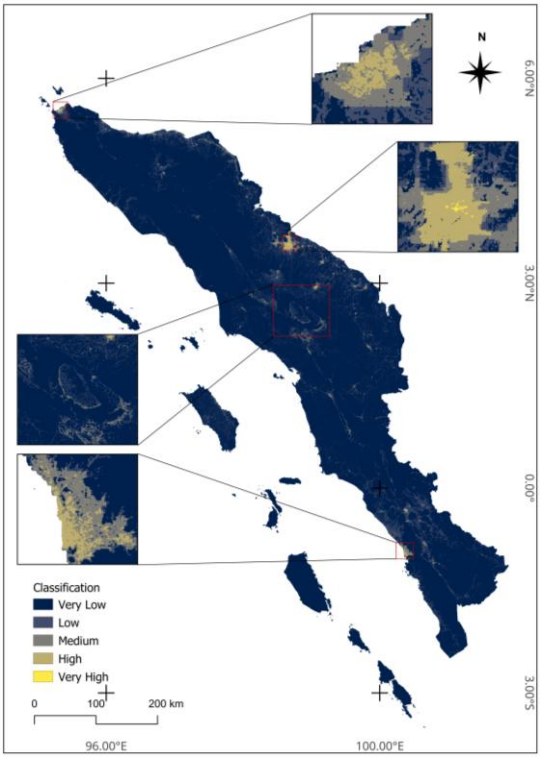

Figure 7. Flood Vulnerability Map Based on Socio-Economic Parameters

The spatial distribution of vulnerability reveals a distinct urban–rural dichotomy. In urban cores, high population density, informal settlements, and a concentration of aging infrastructure intensify exposure, while in densely populated rural agricultural zones, livelihoods tied to flood-sensitive activities such as farming heighten economic vulnerability. The reliance on these zones for food production and economic stability means that flood impacts extend beyond immediate physical damage to long-term food security and economic resilience. This layered vulnerability is not uniformly distributed but is deeply embedded in the socio-economic fabric of specific communities, making targeted interventions essential.

Moreover, the vulnerability map underscores the importance of adaptive capacity. Areas identified with 'Very High' vulnerability not only exhibit high exposure but also demonstrate limited resources for recovery, such as inadequate access to healthcare, financial services, and social safety nets. The interplay between age dependency, economic marginalization, and infrastructural deficits creates a feedback loop that perpetuates vulnerability.

3.3. Integrated Flood Risk and Driver Analysis

The final flood risk map (see Figure 8) was generated through the multiplicative overlay of normalized hazard and vulnerability indices, enabling an integrated assessment of both physical flood processes and socio-demographic susceptibility. Very High-Risk zones occupy approximately 12% of the total study area, representing the critical spatial intersection of the highest hazard (H4–H5) and vulnerability (V4–V5) classes. These zones are predominantly located in low-lying floodplains and densely populated settlements. In these areas, extreme hydrological conditions coincide with limited adaptive capacity, creating concentrated hotspots of potential disaster impact and life-safety risk.

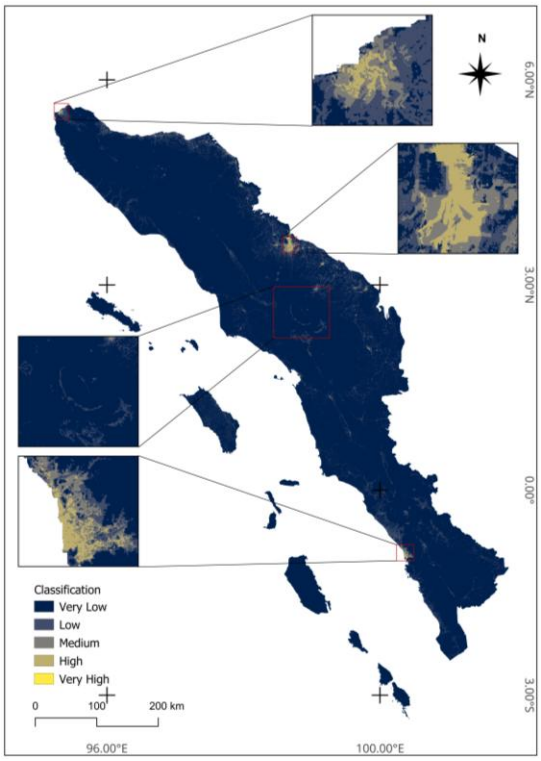

Figure 8. Composite Flood Risk Map

Surrounding these cores, high-risk zone account for an additional 18% of the study area and exhibit more heterogeneous characteristics. These areas are typically defined by either high flood hazard combined with moderate vulnerability, or elevated vulnerability levels under moderate hazard conditions. The spatial continuity between Very High and High-Risk zones highlights transitional risk environments, where incremental changes in hazard intensity or vulnerability can rapidly escalate overall risk levels. This spatial configuration demonstrates that severe flood risk does not arise solely from extreme hazard events or high vulnerability in isolation, but rather from their synergistic interaction, a relationship that is fundamental to the classical risk formulation (Risk = Hazard × Vulnerability). The prominence of such coupling effects in the results is consistent with recent flood risk modeling studies that emphasize hazard–vulnerability integration as a key determinant of flood impacts (Mondal & Garg, 2025; Sigit et al., 2023).

In contrast, extensive Medium Risk zones are primarily distributed across agricultural hinterlands and rapidly developing suburban fringes, where either hazard intensity or vulnerability levels remain moderate. Although the per-unit risk within these areas is lower compared to high-risk zones, their large spatial extent suggests that they may collectively encompass the greatest absolute number of exposed and potentially affected populations. This pattern aligns with recent exposure-oriented flood risk assessments in Southeast Asia, which indicate that moderate-risk regions often contribute disproportionately to total disaster losses due to their spatial scale and population coverage (Jumadi et al., 2024). These findings underscore a critical implication for disaster risk management. While localized Very High-Risk zones necessitate immediate and targeted interventions such as prioritized evacuation planning, structural flood protection, and strict land-use regulation the widespread Medium Risk zones represent a diffuse but equally significant challenge. Addressing risk in these areas requires systematic preparedness strategies, including community-based early warning systems, adaptive livelihood support, and incremental resilience enhancement, to effectively reduce cumulative flood impacts at the regional scale.

3.4. Climatic Drivers: Extreme Rainfall and Tropical Cyclone Influence

A comprehensive analysis of climatological data (2020–2025) reveals significant spatial and temporal anisotropy in precipitation. Figure 9 shows the disparity in monthly precipitation, with maximum accumulation during October–December. Based on the 5-year average, November is the peak of the rainy season, with accumulation reaching 688 mm, statistically significant above other months. The monthly precipitation heatmap (see Figure 10) confirms the most striking positive anomaly occurred in November 2025 (438 mm), coinciding with major flooding. Seasonal patterns, illustrated through LOESS smoothing (see Figure 11), confirm an increasing rainfall trend in the year's final quarter, with widening confidence intervals in November–December reflecting high interannual variability and elevated probability of extremes, consistent with recent findings on rainfall variability in tropical Asia (Nguyen et al., 2023; Ramadhan et al., 2022).

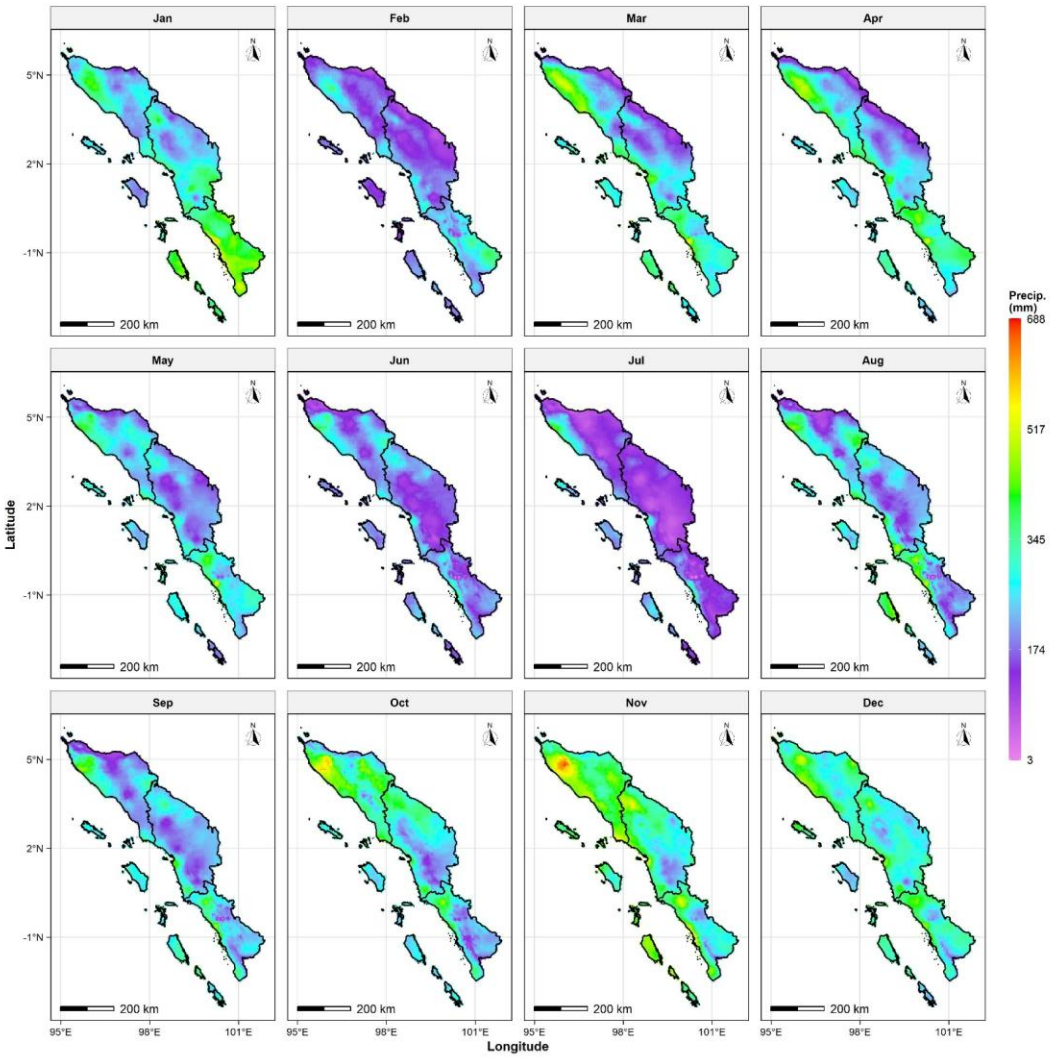

Figure 9. Spatial Distribution of Monthly Mean Precipitation (2020–2025)

Analysis suggests that the November 2025 extreme rainfall event was likely influenced by Tropical Cyclone Senyar (see Figure 12). The cyclone acted as a mesoscale convective catalyst, intensifying low-level convergence, enhancing oceanic moisture transport, and increasing moisture flux convergence over the study area. Interaction with local topography likely amplified orographic lifting, leading to concentrated, high-intensity rainfall.

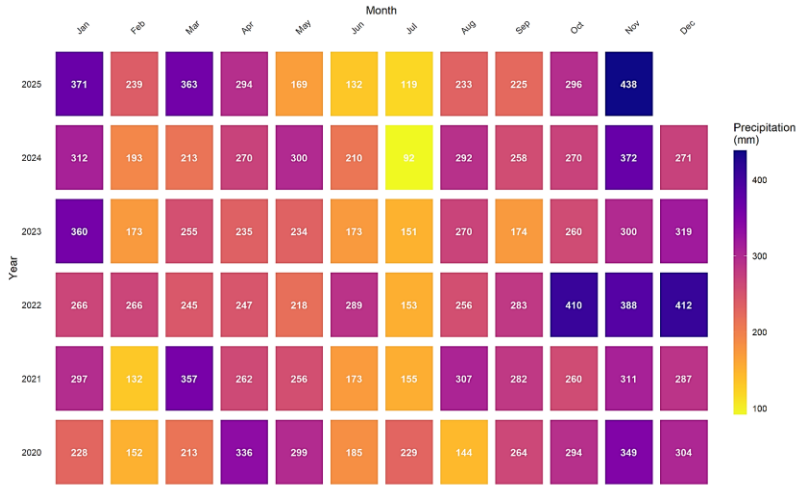

Figure 10. Monthly Precipitation Heatmap (2020–2025)

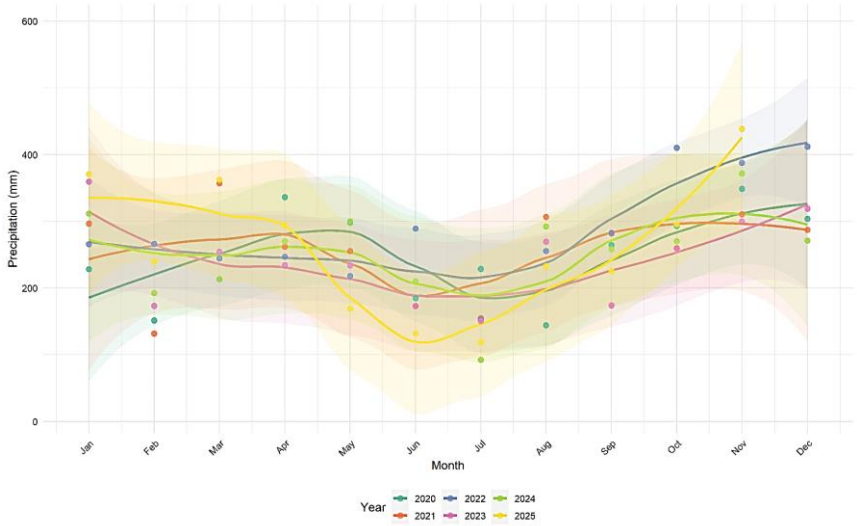

Figure 11. Seasonal Precipitation Patterns with Loess-Smoothed Trends

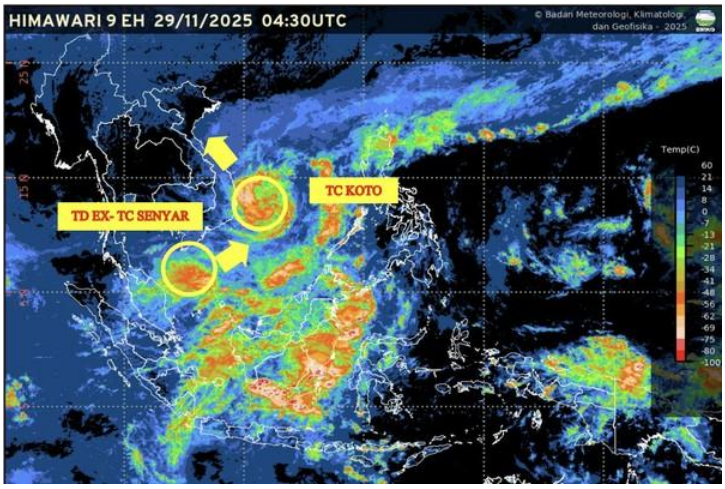

Figure 12. Identification of Tropical Cyclone Senyar (November 2025) from Satellite Observations

These observations suggest that Tropical Cyclone Senyar likely acted as an important synoptic-scale contributing factor that enhanced atmospheric moisture transport and intensified rainfall conditions during the November 2025 flood event. It exemplifies the compound nature of contemporary hydrometeorological hazards, where climate variability (cyclone activity) intersects with local physiography to produce disproportionate impacts, echoing evidence that tropical cyclone–rainfall interactions are intensifying under climate change scenarios (Ariska et al., 2024; Mondal & Garg, 2025). This finding is consistent with operational observations reported by the Indonesian Agency for Meteorology, Climatology, and Geophysics (BMKG, 2025).

3.5. Population Exposure Across Risk Classes

Integration of risk classes with demographic data reveals critical exposure patterns (see Table 4 and Figure 13). While 'Very High Risk' (Risk 4) zones are spatially limited, they define mandatory evacuation areas. The key finding is that 'Medium Risk' (Risk 2) zones encompass the vast majority (87.51% to 97.47%) of the modeled exposed population across the five highest-impact cities. This result carries profound implications for disaster management: the primary humanitarian and logistical challenge likely originate not from the small, highest-risk cores, but from the extensive moderate-risk peripheries where large populations reside. This challenges a common response paradigm focused solely on the most hazardous zones and argues for a strategy that also addresses the extensive "gray zone" of medium risk.

Table 4. Spatial Extent of Flood Risk Classes in High-Impact Cities

City	Model Damaged Area (Ha)			
	Risk 4	Risk 3	Risk 2	Risk 1
North Aceh	10.20	3,511.66	48,720.33	217,345.80
Aceh Tamiang	1.57	635.59	24,620.48	185,593.00
Bireuen	0.00	3,421.86	28,983.43	142,674.60
Gayo Lues	0.00	0.00	3,000.68	551,127.80
Pidie	0.00	3,030.32	21,231.57	283,887.20

Source: Analysis, 2025

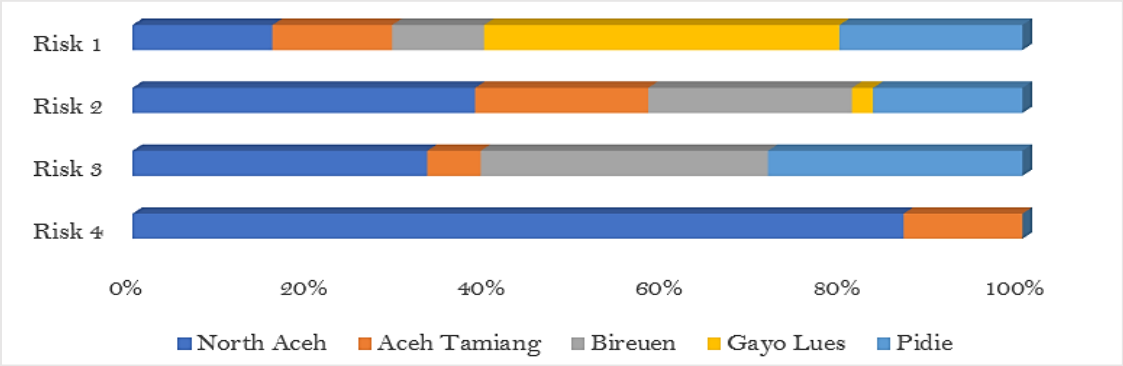

Figure 13. Distribution of Risk Areas for the Five Cities with the Highest Modeled Exposure in Sumatra

3.6. Spatial Correspondence Between Modeled Risk and Observed Flood Impacts

A comparative analysis between modeled flood risk patterns and reported flood impact data from BNPB (National Disaster Management Authority) records as of December 15, 2025, was conducted to assess their spatial correspondence (see Table 5) (BNPB, 2025). In this context, affected population data reflects the combined influence of spatial exposure, settlement distribution, socio-economic vulnerability, and disaster response conditions rather than directly validating flood magnitude or hydrodynamic processes. Therefore, the observed agreement should be interpreted as an indication of the model's ability to capture generalized spatial patterns of potential flood impact.

The comparison indicates that Low Risk zones (Risk 1) contributed minimally to the affected population distribution recorded during the flood events. This aligns with the model's underlying logic, as these zones possess the lowest composite risk scores. The majority of the modeled exposed population was associated with Moderate Risk zones (Risk 2), accounting for 87.51% to 100% of the affected individuals across different regions. This pattern suggests that substantial portions of the affected population were located within spatially extensive intermediate-risk areas. However, the high concentration of affected population within Risk 2 zones may also reflect their broader spatial coverage and settlement extent across the study region. Nevertheless, the observed spatial correspondence provides useful operational insight regarding the distribution of potentially affected populations across different flood risk classes.

Table 5. Validation of Estimated Population Exposure Against Recorded Flood Impacts

City	Population Data Ground Truth		Population Model Damaged/ Total Population (%)			
	Real Damaged (People)	Real Damaged/ Total Population (%)	Risk 1	Risk 2	Risk 3	Risk 4
North Aceh	166,900	26.34	0.00	93.26	6.72	0.02
Aceh Tamiang	159,700	51.43	0.00	97.47	2.52	0.01
Bireuen	39,700	8.57	0.00	89.44	10.56	0.00
Gayo Lues	33,800	31.85	0.00	100	0.00	0.00
Pidie	24,400	5.45	0.00	87.51	12.49	0.00

Source: Analysis, 2025

For instance, in Aceh Tamiang where 51.43% of the population was affected 97.47% of the modeled exposed population was spatially associated with settlements classified as Risk 2. This pattern directly informs intervention strategy, emphasizing that evacuation planning, early warning, and relief efforts should be prioritized for populations in Risk 2, 3, and 4 zones, rather than evenly distributed across all risk categories.

The case of Gayo Lues, where 100% of the modeled exposed population was associated with Risk 2 despite substantial observed impacts, further highlights the influence of localized processes and contextual factors that may not be fully represented within a regional-scale assessment framework. These results suggest that the model is more suitable for identifying generalized spatial patterns and supporting regional-scale prioritization rather than estimating the exact magnitude of flood impacts at highly localized scales. Consequently, the model outputs are best interpreted as decision-support information that should be complemented by local assessments and event-specific observations.

3.7. Deconstructing Risk: The Bivariate Hazard-Vulnerability Matrix

The bivariate hazard–vulnerability framework employed in this study does not introduce a fundamentally new flood risk formulation but rather provides an operational and spatially explicit approach for differentiating dominant flood risk drivers across Sumatra. Unlike conventional composite risk indices that aggregate hazard and vulnerability into a single value, the proposed framework preserves the interaction between both components, thereby improving interpretability and supporting more targeted mitigation prioritization (He et al., 2024; Rahman et al., 2025). This distinction is essential for designing cost-effective mitigation strategies.

The bivariate legend inset in Figure 14 illustrates a 5×5 matrix that categorizes flood risk zones based on the interaction between hazard classes (H1–H5) and vulnerability levels (V1–V5). The matrix reveals five priority zones, each representing a distinct mitigation profile. Zone I (H4–H5 × V4–V5), located in the top-right quadrant, identifies areas of extreme priority where high hazard coincides with high vulnerability. These zones are typically characterized by dense, informal settlements in flood-prone areas with limited coping capacity. Mitigation in these zones must be integrated and multi-dimensional, combining structural flood defenses, permanent evacuation shelters, and prioritization of vulnerable age groups in emergency planning (Dulawan et al., 2024; Rahman et al., 2025).

Zone II (H4–H5 × V1–V2) represents hazard-dominated areas with relatively low vulnerability. These regions require robust hydrological interventions such as real-time rainfall monitoring, early warning systems, and engineered flood control infrastructure (Arrighi et al., 2021; Ibrahim et al., 2024). In contrast, Zone III (H1–H2 × V4–V5) highlights vulnerability-dominated areas where even moderate flooding can result in severe impacts due to demographic sensitivity particularly high concentrations of children and elderly. Non-structural measures such as community preparedness, age-sensitive risk communication, and strengthening of local health and social services are most effective in these contexts (Dulawan et al., 2024). Zone IV (H3–H4 × V3) reflects mixed-driver conditions, often found in peri-urban regions with recurrent flooding and moderate vulnerability. These areas benefit from hybrid approaches that combine localized infrastructure upgrades with social resilience programs. Finally, Zone V (H1–H2 × V1–V2) represents low-priority zones with minimal hazard and vulnerability, where preventive planning and long-term development integration are sufficient.

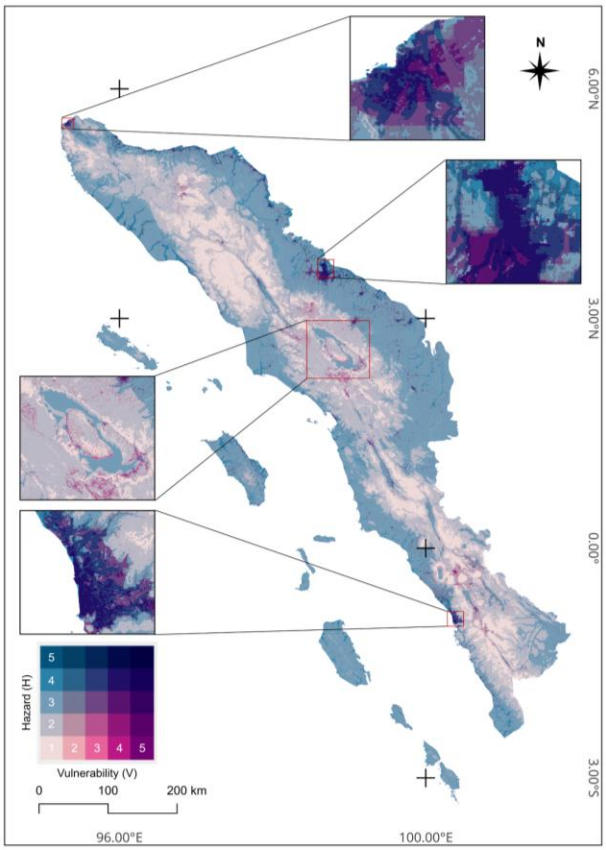

Figure 14. Spatial Delineation of Flood Mitigation Priority Zones

By translating complex spatial data into actionable categories, the bivariate matrix in Figure 14 improves the interpretability of flood risk patterns and supports context-specific mitigation planning. The framework enables the identification of areas where flood risk is predominantly influenced by physical hazard intensity, socio-economic vulnerability, or the interaction between both components. This distinction provides additional decision-support value compared with conventional composite flood risk maps, where hazard and vulnerability are aggregated into a single index. Consequently, the framework may assist planners and disaster management agencies in prioritizing intervention strategies according to local risk characteristics and resource constraints,

3.8. Operational Interpretation of the Bivariate Hazard–Vulnerability Framework

To derive operational insights from the modeled flood risk framework, the flood risk map was integrated with building exposure data and the spatial patterns represented by the 5×5 bivariate hazard–vulnerability

matrix. This synthesis enabled the delineation of context-specific flood mitigation priority zones intended to support strategic and operational flood risk reduction planning (see Table 6). A critical step in this process involved aggregating the 25 hazard–vulnerability combinations into five consolidated priority zones based on dominant risk drivers and key exposure characteristics, including population concentration and critical infrastructure presence.

This aggregation was guided by the dominant risk drivers (i.e., whether risk was primarily hazard-driven, vulnerability-driven, or mixed) and key exposure characteristics, such as population density and the presence of critical infrastructure. This methodological choice significantly enhances interpretability for stakeholders, such as urban planners and emergency managers. Importantly, it achieves this operational simplicity while preserving the analytical detail and diagnostic nuance of the original 5×5 framework. The resulting priority zones showed general spatial consistency with the observed distribution of flood impacts during the November 2025 event.

This prioritized and spatially differentiated approach ensures that limited financial and technical resources are allocated to locations where interventions are most likely to address areas with a high combination of risk and vulnerability, thereby fully aligning with the core principles of risk-informed development and the Sendai Framework's emphasis on understanding risk as a prerequisite for managing it. Consequently, the final spatial representation of these priority zones (see Figure 14) provides a useful operational reference for urban planners, emergency managers, and policymakers. It directly links the diagnostic power of the bivariate hazard-vulnerability analysis to concrete geographical priorities, transforming complex spatial data into a foundational tool for strategic investment, land-use zoning, and community-focused disaster risk reduction planning.

Table 6. Mitigation Priority based on Bivariate Matrix

Priority Zone	Hazard Class	Vulnerability Class	Dominant Risk Driver	Age-Based Vulnerability Pattern	Mitigation & Evacuation Implications
Zone I – Extreme Priority	H4–H5	V4–V5	Hazard + Vulnerability	High proportion of vulnerable age groups (children and elderly) coinciding with very high flood hazard; indicates elevated life-safety risk	Integrated measures: major flood control infrastructure, strict land-use regulation, prioritization of vulnerable age groups in evacuation planning, permanent evacuation shelters
Zone II – High Priority (Hazard-Dominated)	H4–H5	V1–V2	Physical hazard	Lower proportion of vulnerable age groups, but exposed to extreme flood processes	Structural flood mitigation, real-time rainfall monitoring, early warning systems, rapid evacuation with special protocols for elderly and children
Zone III – High Priority (Vulnerability -Dominated)	H1–H2	V4–V5	Age-based vulnerability	High concentration of children and elderly despite relatively low hazard intensity, indicating sensitivity to even moderate flooding	Non-structural measures: community preparedness, targeted evacuation drills, age-sensitive risk communication, strengthening local health and social services
Zone IV – Medium Priority (Mixed Driver)	H3–H4	V3	Hazard and vulnerability balanced	Moderate proportion of vulnerable age groups with recurrent flood exposure	Combined approach: localized drainage improvement, community-based early warning, evacuation planning tailored to vulnerable populations
Zone V – Low Priority	H1–H2	V1–V2	Low hazard and vulnerability	Low proportion of vulnerable age groups and minimal flood exposure	Preventive planning: monitoring demographic changes, maintaining safe evacuation access, integrating flood risk into long-term development

Source: Analysis, 2025

3.9. Uncertainties and Limitations

While the proposed framework provides robust spatial guidance for regional mitigation prioritization, several methodological uncertainties and limitations must be acknowledged. First, this study utilizes an index-based Multi-Criteria Decision Analysis (MCDA) approach. While highly effective for regional-scale spatial prioritization, this method does not simulate hydrodynamic processes such as flood depth, flow velocity, and inundation duration typically captured by mechanistic models (e.g., HEC-RAS). Second, the reliance on the Analytical Hierarchy Process (AHP) introduces inherent subjectivity in the assignment of parameter weights. Although the weights were derived from established literature, future studies should incorporate sensitivity analyses, such as Monte Carlo simulations, to quantify how weight variations influence risk mapping outputs.

Finally, data constraints influenced the spatial representation of vulnerability and hazard. The areal-weighted disaggregation of regency-level demographic data assumes a uniform population distribution within settlement grids, potentially obscuring hyper-local concentrations of vulnerable individuals. Additionally, the hazard model relies on topography and land use as proxies for drainage, as highly granular, sub-surface municipal drainage network data were unavailable for the entire study area. Addressing these data constraints and integrating real-time hydrometeorological forecasting remain important directions for future research.

4. Conclusion

This study developed an integrated flood risk mapping framework for Sumatra, combining multi-parameter hazard assessment with socio-demographic vulnerability analysis and bivariate hazard–vulnerability classification. Results show that High and Very High Hazard zones (21% of study area) concentrate in lowland river basins, strongly correlated with extreme November 2025 rainfall (438 mm) amplified by Tropical Cyclone Senyar. Key findings reveal that medium-risk (Risk 2) zones account for 87–97% of exposed populations across major cities, indicating that flood impacts extend far beyond limited high-risk cores. Comparison with reported flood impact data indicates general spatial correspondence between modeled flood risk patterns and the distribution of affected populations, particularly within the spatially extensive medium-risk (Risk 2) zones in Aceh Tamiang. The 5×5 bivariate hazard–vulnerability matrix enables differentiated mitigation prioritization: extreme-risk zones (high hazard-high vulnerability) require integrated structural-social measures; hazard-dominated zones need engineered defenses and early warning; vulnerability-dominated zones benefit most from community preparedness and social protection. This framework provides an interpretable framework for differentiating mitigation priorities according to the relative dominance of hazard intensity and socio-economic vulnerability. Rather than replacing conventional composite flood risk indices, the framework complements them by supporting more context-specific and operationally targeted flood mitigation planning.

5. Acknowledgments

The authors would like to express their sincere gratitude to all relevant stakeholders for their provision of the secondary datasets used in this study. This research was supported by the Directorate General of Higher Education, Research, and Technology (Ditjen Dikti), Ministry of Education, Culture, Research, and Technology of the Republic of Indonesia, through the PMDSU Research Program.

6. References

Aeni, P., & Anwar, K. M. (2024). Hydrometeorological Disaster: Challenges and Mitigation in Indonesia. *Jurnal Indonesia Sosial Teknologi, 5*(01), 318–330. [Crossref]

Ahmed, I., Das (Pan), N., Debnath, J., Bhowmik, M., & Bhattacharjee, S. (2024). Flood hazard zonation using GIS-based multi-parametric Analytical Hierarchy Process. *Geosystems and Geoenvironment, 3*(2). [Crossref]

Ali, S. A., Khatun, R., Ahmad, A., & Ahmad, S. N. (2019). Application of GIS-based analytic hierarchy process and frequency ratio model to flood vulnerable mapping and risk area estimation at Sundarban region, India. *Modeling Earth Systems and Environment, 5*(3), 1083–1102. [Crossref]

Ariska, M., Suhadi, Supari, Irfan, M., & Iskandar, I. (2024). Spatio-Temporal Variations of Indonesian Rainfall and Their Links to Indo-Pacific Modes. *Atmosphere*, *15*(9). [Crossref]

Ariyani, D., Purwanto, M. Y. J., Sunarti, E., Perdinan, & Juniati, A. T. (2024). Integrated flood hazard assessment using multi-criteria analysis and geospatial modeling. *Journal of Degraded and Mining Lands Management*, *11*(4), 6121–6134. [Crossref]

Arrighi, C., Pregnolato, M., & Castelli, F. (2021). Indirect flood impacts and cascade risk across interdependent linear infrastructures. *Natural Hazards and Earth System Sciences*, *21*(6), 1955–1969. [Crossref]

Asaaga, F. A., Purse, B. V., Rahman, M., Srinivas, P. N., Kalegowda, S. D., Seshadri, T., Young, J. C., & Oommen, M. A. (2023). The role of social vulnerability in improving interventions for neglected zoonotic diseases: The example of Kyasanur Forest Disease in India. *PLOS Global Public Health*, *3*(2), 1–28. [Crossref]

Badan Meteorologi Klimatologi dan Geofisika (BMKG). (2025). *Citra Himawari-9 IR Enhanced – Indonesia*. BMKG. https://www.bmkg.go.id/cuaca/satelit/himawari-ir-enhanced

Badan Nasional Penanggulangan Bencana (BNPB). (2025). *Rekapitulasi Terdampak Bencana Sumatera 2025*. BNPB Geoportal. https://gis.bnpb.go.id/BANSORSUMATERA2025/

Bui, D. T., Ngo, P. T. T., Pham, T. D., Jaafari, A., Minh, N. Q., Hoa, P. V., & Samui, P. (2019). A novel hybrid approach based on a swarm intelligence optimized extreme learning machine for flash flood susceptibility mapping. *Catena*, *179*(October 2018), 184–196. [Crossref]

de Ruiter, M. C., Couasnon, A., van den Homberg, M. J. C., Daniell, J. E., Gill, J. C., & Ward, P. J. (2020). Why We Can No Longer Ignore Consecutive Disasters. *Earth's Future*, *8*(3). [Crossref]

Diriba, D., Takele, T., Karuppannan, S., & Husein, M. (2024). Flood hazard analysis and risk assessment using remote sensing, GIS, and AHP techniques: a case study of the Gidabo Watershed, main Ethiopian Rift, Ethiopia. *Geomatics, Natural Hazards and Risk*, *15*(1). [Crossref]

Dulawan, J. M. T., Imamura, Y., Konishi, T., Amaguchi, H., & Ohara, M. (2024). A systematic framework for assessing social vulnerability to flood for integrated flood risk management: A case study in Metro Manila, Philippines. *International Journal of Disaster Risk Reduction*, *112*(August), 104778. [Crossref]

Ekmekcioğlu, Ö., Koc, K., & Özger, M. (2021). District based flood risk assessment in Istanbul using fuzzy analytical hierarchy process. *Stochastic Environmental Research and Risk Assessment*, *35*(3), 617–637. [Crossref]

European Commission. (2025). *Indonesia, Thailand, Malaysia | Severe weather and floods - DG ECHO Daily Map | 18/12/2025*. Reliefweb. https://reliefweb.int/map/indonesia/indonesia-thailand-malaysia-severe-weather-and-floods-dg-echo-daily-map-18122025

Ferreira, T. M. (2020). Recent advances in the assessment of flood risk in urban areas. *Water (Switzerland)*, *12*(7), 10–12. [Crossref]

Gomez Vaca, A. N., Popartan, L. A., Nuss-Girona, S., & Rodríguez-Roda, I. (2025). Spatial approach for assessing vulnerability to urban flooding: a proposal for a multidimensional index. *Natural Hazards*, *121*(14), 16799–16825. [Crossref]

He, L., Li, Q., Zhang, J., Deng, X., Wu, Z., Wang, Y., Chan, P. W., & Li, N. (2024). Enhanced Tropical Cyclone Precipitation Prediction in the Northwest Pacific Using Deep Learning Models and Ensemble Techniques. *Water (Switzerland)*, *16*(5). [Crossref]

Ibrahim, M., Huo, A., Ullah, W., Ullah, S., & Xuantao, Z. (2024). An integrated approach to flood risk assessment using multi-criteria decision analysis and geographic information system. A case study from a flood-prone region of Pakistan. *Frontiers in Environmental Science*, *12*(January), 1–16. [Crossref]

Intergovernmental Panel on Climate Change (IPCC). (2023). Climate Change 2021 – The Physical Science Basis. In *Climate Change 2021 – The Physical Science Basis*. [Crossref]

Islam, T., Zeleke, E. B., Afroz, M., & Melesse, A. M. (2025). A Systematic Review of Urban Flood Susceptibility Mapping: Remote Sensing, Machine Learning, and Other Modeling Approaches. *Remote Sensing*, *17*(3). [Crossref]

Istiawan, D., Wulandari, R., & Sulastri. (2023). Mapping of Social Vulnerability to Natural Hazards in Geodemographic Analysis Using Fuzzy Geographically Weighted Clustering. *Scientific Journal of Informatics*, *10*(4), 413–422. [Crossref]

Jumadi, J., Danardono, D., Priyono, K. D., Roziaty, E., Masruroh, H., Rohman, A., Amin, C., Hadibasyir, H. Z., Fikriyah, V. N., Nawaz, M., Sattar, F., & Lotfata, A. (2024). Utilizing Open Access Spatial Data for Flood Risk Mapping: A Case Study in the Upper Solo Watershed. *Geoplanning*, *11*(2), 189–204. [Crossref]

Lanlan, J., Sarker, M. N. I., Ali, I., Firdaus, R. B. R., & Hossin, M. A. (2024). Vulnerability and resilience in the context of natural hazards: a critical conceptual analysis. *Environment, Development and Sustainability*, *26*(8), 19069–19092. [Crossref]

Leal, M., Reis, E., Pereira, S., & Santos, P. P. (2021). Physical vulnerability assessment to flash floods using an indicator-based methodology based on building properties and flow parameters. *Journal of Flood Risk Management*, *14*(3), 1–19. [Crossref]

Magnini, A., Lombardi, M., Bujari, A., Mattivi, P., Shustikova, I., Persiano, S., Patella, M., Bitelli, G., Bellavista, P., Lo Conti, F., Tirri, A., Bagli, S., Mazzoli, P., & Castellarin, A. (2023). Geomorphic flood hazard mapping: from floodplain delineation to flood hazard characterization. *Hydrological Sciences Journal*, *68*(16), 2388–2403. [Crossref]

Megahed, H. A., Abdo, A. M., AbdelRahman, M. A. E., Scopa, A., & Hegazy, M. N. (2023). Frequency Ratio Model as Tools for Flood Susceptibility Mapping in Urbanized Areas: A Case Study from Egypt. *Applied Sciences (Switzerland)*, *13*(16). [Crossref]

Mondal, A., & Garg, R. D. (2025). Global urban flood dynamics and future vulnerability assessment: a comprehensive study of trends, predictions, and mitigation. *Natural Hazards*, *121*(9), 11187–11207. [Crossref]

Nguyen, D. L., Chou, T. Y., Hoang, T. V., & Chen, M. H. (2023). Flood Susceptibility Mapping Using Machine Learning Algorithms: A Case Study in Huong Khe District, Ha Tinh Province, Vietnam. *International Journal of Geoinformatics*, *19*(7), 1–15. [Crossref]

Pakati, S. S., Shoko, C., & Dube, T. (2025). Integrated flood modelling and risk assessment in urban areas: A review on applications, strengths, limitations and future research directions. *Journal of Hydrology: Regional Studies*, *61*(July), 102583. [Crossref]

Parizi, S. M., Taleai, M., & Sharifi, A. (2022). A GIS-Based Multi-Criteria Analysis Framework to Evaluate Urban Physical Resilience against Earthquakes. *Sustainability (Switzerland)*, *14*(9). [Crossref]

Parsian, S., Amani, M., Moghimi, A., Ghorbanian, A., & Mahdavi, S. (2021). Flood hazard mapping using fuzzy logic, analytical hierarchy process, and multi-source geospatial datasets. *Remote Sensing*, *13*(23). [Crossref]

Purwanto, A., Rustam, Eviliyanto, & Andrasmoro, D. (2022). Flood Risk Mapping Using GIS and Multi-Criteria Analysis at Nanga Pinoh West Kalimantan Area. *Indonesian Journal of Geography*, *54*(3), 463–470. [Crossref]

Rahman, M. M., Tanni, K. N., Shobuj, I. A., Hossain, M. T., Alam, E., Al Hattaw, K. S., & Islam, M. K. (2025). Multidimensional Vulnerability Assessment for Floods: Evidence From Flood-Prone Areas of Bangladesh. *Journal of Flood Risk Management*, *18*(3). [Crossref]

Ramadhan, R., Marzuki, M., Suryanto, W., Sholihun, S., Yusnaini, H., Muharsyah, R., & Hanif, M. (2022). Trends in rainfall and hydrometeorological disasters in new capital city of Indonesia from long-term satellite-based precipitation products. *Remote Sensing Applications: Society and Environment*, *28*(July), 100827. [Crossref]

Rufat, S., Tate, E., Emrich, C. T., & Antolini, F. (2019). How Valid Are Social Vulnerability Models? *Annals of the American Association of Geographers*, *109*(4), 1131–1153. [Crossref]

Saha, A., Pal, S. C., Arabameri, A., Blaschke, T., Panahi, S., Chowdhuri, I., Chakrabortty, R., Costache, R., & Arora, A. (2021). Flood susceptibility assessment using novel ensemble of hyperpipes and support vector regression algorithms. *Water (Switzerland)*, *13*(2), 1–27. [Crossref]

Sakti, A. D., Deliar, A., Hafidzah, D. R., Chintia, A. V., Anggraini, T. S., Ihsan, K. T. N., Virtriana, R., Suwardhi, D., Harto, A. B., Nurmaulia, S. L., Aritenang, A. F., Riqqi, A., Hernandi, A., Soeksmantono, B., & Wikantika, K. (2024). Machine learning based urban sprawl assessment using integrated multi-hazard and environmental-economic impact. *Scientific Reports*, *14*(1), 1–16. [Crossref]

Santi, H., Ginting, B., Sitorus, H., Ismail, R., & Manurung, R. (2022). Social Capital in Mitigating Flood Disaster in the People of Aceh Tenggara, Indonesia. *Open Access Indonesia Journal of Social Sciences*, *5*(3), 758–764. [Crossref]

Sigit, A., Koyama, M., & Harada, M. (2023). Flood Risk Assessment Focusing on Exposed Social Characteristics in Central Java, Indonesia. *Sustainability (Switzerland)*, *15*(24). [Crossref]

Taoukidou, N., Karpouzos, D., & Georgiou, P. (2025). Flood Hazard Assessment Through AHP, Fuzzy AHP, and Frequency Ratio Methods: A Comparative Analysis. *Water (Switzerland)*, *17*(14). [Crossref]

Tellman, B., Sullivan, J. A., Kuhn, C., Kettner, A. J., Doyle, C. S., Brakenridge, G. R., Erickson, T. A., & Slayback, D. A. (2021). Satellite imaging reveals increased proportion of population exposed to floods. *Nature*, *596*(7870), 80–86. [Crossref]

Verma, P., Khan, A. S., & Safiullah, Z. N. A. (2025). Urban Flood Resilience in India: A Comprehensive Review of Challenges, Assessment Strategies, and Future Directions. *Journal of Environment and Bio-Science*, *39*(01), 69. [Crossref]